NJC

Accepted Manuscript

This is an *Accepted Manuscript*, which has been through the Royal Society of Chemistry peer review process and has been accepted for publication.

Accepted Manuscripts are published online shortly after acceptance, before technical editing, formatting and proof reading. Using this free service, authors can make their results available to the community, in citable form, before we publish the edited article. We will replace this *Accepted Manuscript* with the edited and formatted *Advance Article* as soon as it is available.

You can find more information about *Accepted Manuscripts* in the **Information for Authors**.

Please note that technical editing may introduce minor changes to the text and/or graphics, which may alter content. The journal's standard **Terms & Conditions** and the **Ethical guidelines** still apply. In no event shall the Royal Society of Chemistry be held responsible for any errors or omissions in this *Accepted Manuscript* or any consequences arising from the use of any information it contains.

Journal Name
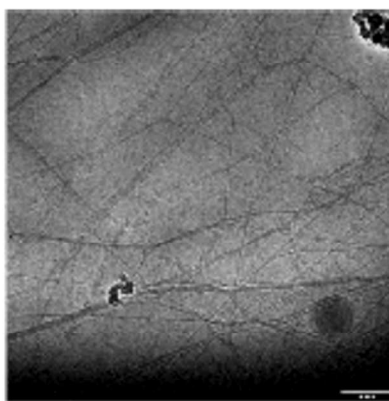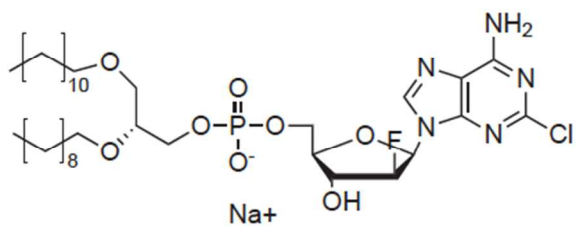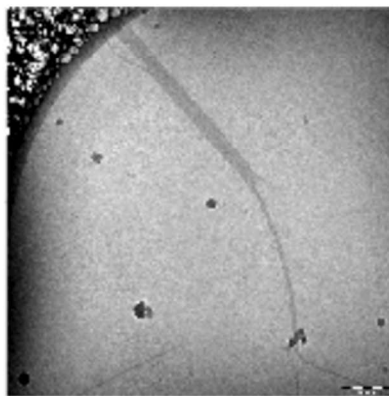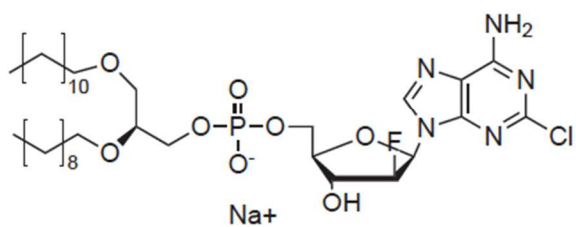
ARTICLE

Diastereoselective Self-Assembly of Clofarabine Lipids

Peter Sandin,[+,a,b] Francesca Baldelli Bombelli,[+,a,c,d] Benedetta Castroflorio,[a] Christoph Müller,[e] Jürgen Obermeier,[e] Göran Karlsson,[f] Katarina Edwards,[f] Piero Baglioni[a] and Debora Berti[*a]

Clofarabine is a nucleosidic chemotherapeutic approved for the treatment of acute lymphoblastic leukemia, currently undergoing clinical trials for the treatment of solid tumors. Like for many other, a lipidic derivatization of this drug improves pharmacokinetics and relieves the heavy side effects. Since the self-assembly pattern can modulate the bioactivity profile, a precise knowledge of the aggregation behavior of these nucleolipids and of the microstructure of the aggregates is central to design formulations that efficiently provide sufficient bioavailability. In this contribution we investigate the self-assembly behavior of two Clofarabine dioxy-ether derivatives, the diastereomeres (1-2S and 1-2R). . These Clofarabine lipid derivatives showed an unexpected diastereoselective self-assembly effect, which we have monitored observing the time evolution of self-assemblies and their microstructural response to thermal treatments. Dynamic Light Scattering and Circular Dichroism provide an ensemble of results which correlate with the occurrence of a hierarchical association of wormlike aggregates, imaged with Electron Microcopy. A strikingly different behavior for the two diastereomers was observed. This behavior can be crucial for the different bioavailability observed *in vivo*.

Journal Name

ARTICLE

Introduction

Clofarabine is a cytotoxic deoxyadenosine analogue that received accelerated approval in 2004 from FDA[1] and recently from EMEA[2] for the treatment of pediatric acute lymphoblastic leukemia, currently under clinical trials for some adult solid tumors.[3]

A dose-dependent severe myelosuppression represents its most serious side-effect.[4] Like for many other nucleosidic chemotherapeutics, a pro-nucleotide approach,[5] with a specific lipid carrier linked to the nucleoside via a covalent phosphodiester bond, can reduce these effects, improve pharmacokinetic behavior and overcome or decrease the development of resistance against the drug.

Recently we have synthesized a specific conjugate of clofarabine with a synthetic dialkyl lipid phosphate, (1, Fig. 1), which showed improved pharmacokinetic, pharmacodynamic and toxicologic properties compared to free clofarabine.[6]
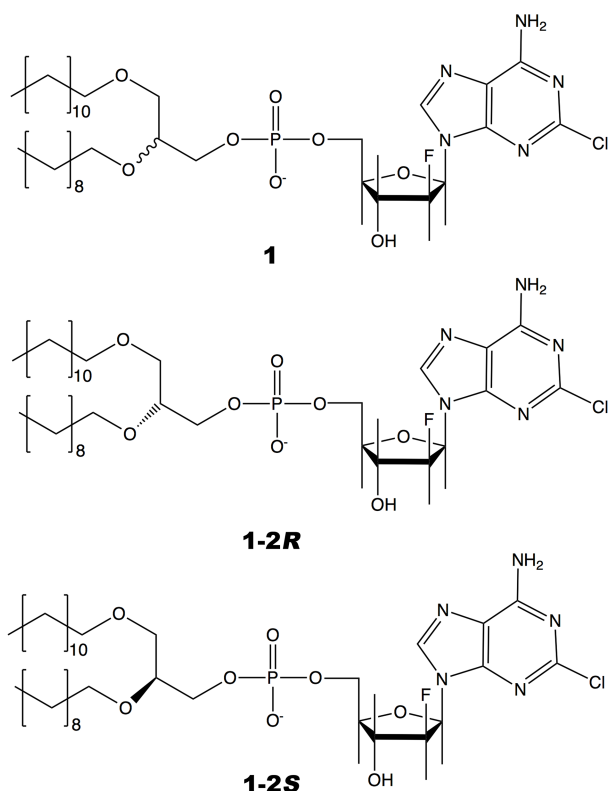
Fig. 1 Chemical structures of 1 and its diastereomers 1-2*R* and 1-2*S*.

In vivo 1 is activated by membrane associated specific

hydrolases, releasing the free clofarabine into the respective cells. Since 1 is a 1:1 mixture of two diastereomeres (1-2S and 1-2R, Fig. 1), the question arose whether the two diastereomers would differ with regard to biological activity, with the 1-2R, sterically similar to natural phospholipids, expected to be the most active. For this reason we synthesized 1-2S and 1-2R. Remarkably, 1-2S, with the "unnatural" S configuration at carbon sn2 in the lipid part, showed higher bioavailability and anti-tumor activity *in vivo*.[6] The stereochemical difference involves a portion of the molecule, which is cleaved away from the active clofarabine part, and should in principle have little effect on biological properties. The reasons for the observed difference in bioactivity must therefore lay elsewhere. The amphiphilic properties of 1-2R and 1-2S suggest the possibility of aggregation and formation of ordered supramolecular structures in solution. Amphiphilic self-assemblies display a rich phase behavior, characterized by a large structural diversity, in terms of size, shape and flexibility of the aggregates. The typical independent parameters of amphiphilic phase diagram are surfactant volume fraction, temperature and ionic strength: subtle variations of local microstructure can lead to cascade effects with dramatic morphological transitions on the mesoscale.[7] This effect is particularly important for biologically-inspired functional surfactants, such as peptide-amphiphiles and oligonucleotide-amphiphiles,[8-11] where a biological recognition unit is incorporated in the amphiphile molecular architecture.

This paper investigates the self-assembly behavior displayed by clofarabine lipid diasteromers reported in Fig. 1, which could influence their biological activity.

A diastereoselective assembly is by no means obvious for ionic amphiphiles, because predictions on the morphology of the aggregate are based on the balance of molecular packing parameters and excluded volume or electrostatic repulsive interactions between the polar heads. Therefore, a different stereochemistry at the C2 should in principle play little or no role on the structural properties of the aggregates.

On the other side, lipophilic nucleosides are known to give rise to interesting and extremely rich phase behavior in aqueous solutions. Clofarabine is a derivative of adenosine and we have previously studied the aggregation behavior of Phosphatidyl-Nucleosides, where a natural RNA nucleotide is conjugated to a double-chain glycerol lipid skeleton. These derivatives self-organize in aqueous solution as assemblies of various size, shape and interfacial curvature, according on the length of the two hydrophobic portions.[12,13] The nucleic motif imparts molecular recognition capability to self-assemblies A coarse-grained mapping of the phase behavior in aqueous solutions can be predicted by comparison with the corresponding

phosphatidylcholine precursors[14]: as the hydrophobic double chain is lengthened, the dimensionless surfactant packing parameter $p= v/a_0 l_c$, with v the volume of the alkyl chain, a_0 the cross section of the polar head and l_c the fully extended length of the hydrophobic portion, increases until it reaches an asymptotic value. In this progression, we observed the usual phase evolution, from positively curved surfactant films (globular micelles) to flat assemblies (bilayers). However, since the geometry of spontaneous self-assembly and interfacial film properties are the result of delicate balance between hydrophobic forces and polar head interactions, the properties of nucleolipid self-assemblies is further modulated by base-base interactions, that are triggered by aggregation.[15] Their self-assemblies show a strong dependence on subtle changes of molecular details of the monomer, such as the *syn* or *anti* conformation of the nucleoside. Some reports on amphiphiles with functional polar heads have shown that, when a complex interaction pattern at the intra- and inter-aggregate level can occur at the interface, variations in the stereochemistry of the polar head, of the counterions, or slight changes in the experimental conditions, can promote drastic alterations of the aggregate morphology.[17-19] An illuminating example is provided by dilauroyl-phosphatidyl-N (DLPN), with N either adenosine or uridine, whose aggregation properties have been studied in detail, to better highlight the contribution of the functional polar head to local and mesosocopic properties of the aggregates. Freshly prepared dilauroyl-phosphatidyl-Adenosine solutions are mostly composed of threadlike flexible micelles whose cross-section size is about 5 nm. The observed time evolution of the aggregate morphology results in twisted superstructures, which account for the appearance of an ultraslow relaxation in quasielastic light scattering. Conversely DLPU forms wormlike flexible micelles, whose structure is stable with time and which do not associate into superstructures. DLPA superstructures arise from the hierarchical aggregation of wormlike structures identical to dilauroyl-phosphatidyl-uridine micelles. The higher stacking constant of the former nucleotide is responsible for the different self-assembly behavior, which is also strictly dependent on the thermal history of the samples, which alters the syn–anti distribution of conformers of the adenosine headgroups. The syn-anti redistribution is then retained when the sample is brought back to room temperature, due to the intermolecular constraints present in the self-assembled structure.[20]

In this contribution we focus on an even subtler aspect, i.e. the stereochemistry of the polar head at the sn2 carbon. If base-base associative interactions at the polar head level are operative, then despite the same charge of the headgroups, the stereochemical details may have a deep influence on the self-assembly and on the hierarchical assembly of associated units.

To address this issue, we compare the microstructure of the aggregates formed by 1-2R and 1-2S.

We expect the local structure to be similar to the DLPN case, i.e. that the amphiphiles will assemble into locally cylindrical micelles. Any difference of the flexibility of the aggregates, and the association of simpler associated units into hierarchical super- twisted super structures, should be ascribed to the specificity of the polar head and to the effect that the stereochemistry of the sn2 Carbon has on the interaction pattern.

Materials and methods

Synthesis and characterization of the diastereomers

The preparation of [2-Chloro-9-(2'-deoxy-2'-fluoro-β-D-arabinofuranosyl) adenine]-5'-phosphoric acid-(2R-decyloxy-3-dodecyloxy)propyl ester (1-2R) is shown in Scheme 1.
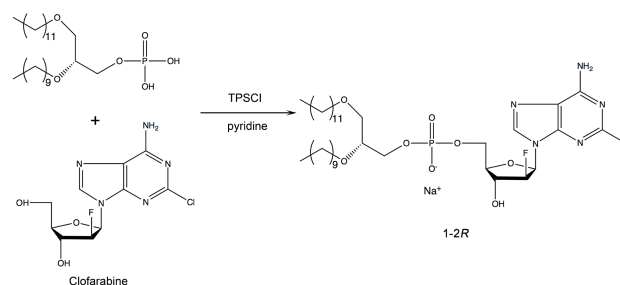
Scheme 1 Synthetic pathway to the diastereomer 1-2R.

All the reagents, chemicals and solvents have been purchased from Sigma Aldrich and used without further purification.

4.41 g (9,17 mmol) of enantiomerically pure phosphoric acid-(2R-decyloxy-3-dodecyoxo-) propyl ester, synthesised from (S)-(+)-1,2-Isopropylideneglycerol as previously described,[21] are treated twice with 50 ml of anhydrous pyridine and concentrated by evaporation. The residue is dissolved in 180 ml of anhydrous pyridine at room temperature, treated with 5.56 g (18.35 mmol) of 2,4,6-triisopropylbenzenesulfonyl chloride under nitrogen and stirred at 20-25°C for 1 hour. Then 4.18 g (13.76 mmol=1.5 eq.) of 2-chloro-9-(2'-deoxy-2'-fluoro arabinofuranosyl) adenine (Clofarabine) are added at once, and the mixture is stirred under nitrogen for 20 hours. Hydrolysis is performed by adding 100 ml of saturated sodium hydrogencarbonate solutio;, the mixture is stirred for another 0.5 hour at room temperature until ending of carbon dioxide evolution and freed from solvent under vacuum at 40°C. Acetone (150 ml) is added to the solid residue vigorously stirred for an additional hour. The resulted suspension is filtrated with suction and the residual salt is washed with 50 ml acetone. The combined acetone filtrate and washings are concentrated and the residue is purified by HPLC on Lichrospher 60 RPselect B with methanol/aqueous 40mM sodium acetate 85:15 as the eluent. The product containing fractions are evaporated. The residue is distributed between 200 ml of tert-butylmethylether and 60 ml of 2N hydrochloric acid. The organic layer is evaporated, the residue is dissolved in a mixture of 20 ml of methanol and the pH is adjusted to pH 7 by addition of sodium methanolate (30 % in methanol). The solvent is stripped of and the residual sodium salt dissolved in 25 ml acetone and dropped at 0°C to 50 ml acetonitrile. The resulting suspension is stirred for 1 h at 0°C, the precipitate is filtered off with suction washed with 50 ml ice cold acetonitrile

and dried in vacuum: 5.50 g (76 %) sodium salt of 1-2R as white amorphous powder.

^{1}H NMR. (300 MHz, DMSO-d$_6$): 8.2 (s, 1H, H$_8$), 8,0, (s (br), 1H, NH$_2$), 6,6, (s, 1H, 3'-OH), 6.3 (dd, 1H, H$_{1'}$), 5.2 (dt, 1H, H$_{2'}$), 4.5, (dt, 1H, H$_{3'}$), 3.9-4.0, (m, 3H, H$_{4'}$, POCH$_2$), 3.6, (m, 1H, -H$_{5a'}$), 3.6 (m, 1H, H$_{5'b}$), 3.2-3.5 (m, 7H, >CHOCH$_2$-, -CH$_2$OCH$_2$), 1.1-1.4 (m, 32H, -(CH$_2$)$_9$-, -(CH$_2$)$_7$-), 0.8 (m, 6H, CH$_2$-CH$_3$); $^3J_{1'-H,2'-H} \approx {}^3J_{2'-H,3'-H} \approx {}^3J_{3'-H,4'-H} \approx 4.6$ Hz, $^3J_{1'-H,F} = 13.2$ Hz, $^2J_{2'-H,F} = 52,7$ Hz, $^3J_{3'-H,F} = 19.4$ Hz.

^{13}C NMR- (75,0 MHz, DMSO-d$_6$): 156.6, 153.1, 150.0 (C-2, C-4, C-6), 139.7 (C-8), 117.2 (C-5), 95.8+ 93.9 (C-2'), 82,0 (C-4'), 81.2 (C-1'), 77,7 (O-CH<), 73,1 (C-3'), 70.7, 70.4 (CH$_2$-CH$_2$O-CH$_2$-), 69.1 (CH$_2$-CH$_2$O-CH<), 63.6 (C-5'), 63.3 (5'-O-P(O)$_2$OCH$_2$), 21,8-31,1 (-(CH$_2$)$_9$-, -(CH$_2$)$_7$-), 13.6 (2× CH$_3$)

^{31}P NMR (121,5 MHz, DMSO-d$_6$): 0,23 ppm (singlet).

^{19}F NMR (282 MHz, DMSO-d$_6$): -199.5 ppm (singlet $-^1$H-decoupled).

Mass spec. (FAB–): m/z = 764.39 [M-Na$^+$]

The preparation of [2-Chloro-9-(2'-deoxy-2'-fluoro-β-D-arabinofuranosyl)adenine]-5'-phosphoric acid-(2S-decyloxy-3-dodecyloxy)propyl ester (1-2S) is similar to what reported for 1-2R, except for the use of enantiomerically pure phosphoric acid-(2S-decyloxy-3-dodecyloxoy)propyl ester (synthesised from (R)-(-)-1,2-Isopropylideneglycerol as in WO 96/06620). 1-2S is obtained as sodium salt in 28 % yield.

^{19}F NMR (282 MHz, , DMSO-d$_6$): -198.5 ppm (singlet $-^1$H-decoupled).

Dynamic Light Scattering (DLS)

DLS experiments were carried out on a Brookhaven Instrument apparatus, New York, USA (BI 9000AT correlator card and BI 200 SM goniometer). The signal was detected by an EMI 9863B/350 photomultiplier. The light source was the doubled frequency of a Coherent Innova diode pumped Nd-YAG laser, (λ = 532 nm, 20 mW. The laser long term power stability was ± 0.5%. Self-beating detection was recorded using decahydronaphthalene (thermostated by a water circulating system) as index matching liquid. A temperature probe was inserted in the sample to monitor T while simultaneously recording autocorrelation functions. Measurements have been performed at 20°C on 0.5 ml samples previously transferred into cylindrical Hellma scattering cells. For each sample at least three separate measurements were performed at different angles (i.e. 70^0, 90^0, 120^0) corresponding to three different scattering vectors; n is the refractive index of the medium equal to 1.33. In Dynamic Light Scattering experiments, the normalized time autocorrelation function $g_2(q,t)$ of the scattered intensity is measured according to:

$$g_2(q,t) = \frac{\langle I^*(q,0)I(q,t)\rangle}{\langle I(q,0)^2\rangle} \qquad 1)$$

For ergodic systems, this function can be expressed in terms of the field autocorrelation function $g_1(q,t)$ through the Siegert relation:

$$g_2(q,t) = A\left[1 + \beta^2 g_1(q,t)^2\right] \quad 2)$$

where A is the baseline and β^2 is the coherence factor dependent on the scattering geometry and details of the detection system.

Data analysis has been performed by fitting the field autocorrelation functions through a double exponential decay, yielding two distinct decay rates, labeled as "fast" and "slow" decay modes. The analytical expression used to fit the field autocorrelation functions was:

$$g_1(q,t) = A\left(Pe^{-\Gamma_1 t} + (1-P)e^{-\Gamma_2 t}\right) + B \qquad 3)$$

where A is the total amplitude of the correlation function, P is the contribution of the first mode to the total amplitude, B is the baseline. The extracted decay modes have a typical diffusive scaling: it is commonly agreed that a linear dependence of the decay rate on the square scattering vector, q^2, indicates a diffusive origin (Fig. 2). The line slope is the translational diffusion coefficient D_t of that population. The diffusion coefficients provide access to the hydrodynamic correlation lengths R_H for isotropic particles through the Stokes-Einstein relationship

$$D_t = \frac{k_B T}{6\pi\eta_s R_H} \qquad 4)$$

where η_S is the solvent viscosity and k_B the Boltzmann constant. Although such hydrodynamic sizes cannot be related to any structural parameter of anisotropic particles, as they refer to the radius of the equivalent diffusing spheres, can qualitatively indicate the order of magnitude of the size of the diffusing self-assemblies.
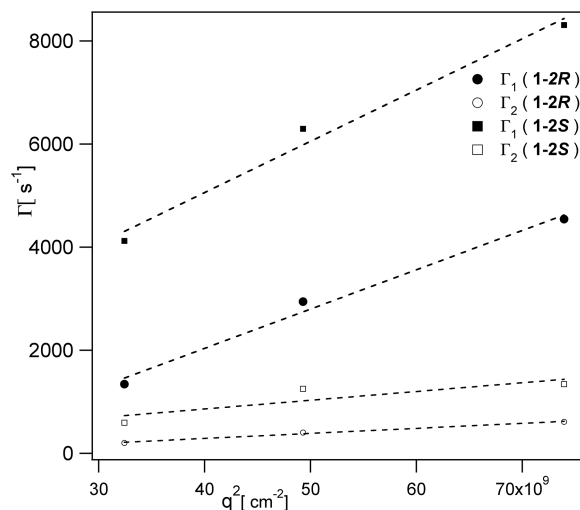
Fig. 2 Decay modes, extracted from the field autocorrelation functions through equation 3, are reported as a function of the squared scattering vector q. Γ_1 and Γ_2 are the fast and slow decay mode, respectively. The linear dependence of the

decay rate on the squared scattering vector, q^2, indicates a diffusive nature of both decays. The values of the diffusion coefficients are shown in Table 1

Circular Dichroism Spectroscopy (CD)

Circular Dichroism spectra were collected on a J-715 Jasco spectro-polarimeter. Hellma quartz cylindrical cells with variable path-length, selected not to exceed 0.8 optical density, were used. The observed circular dichroism was converted into Molar Ellipticity, normalizing for pathlength and dichroic chromophore concentration.

Cryo-transmission electron microscopy (Cryo-TEM)

The preparation of the samples for Cryo-TEM was performed as follows: a small droplet of the solution was placed under controlled conditions on a pretreated 20 μm thick Cu grid, coated with a perforated cellulose acetate butyrate film. The excess material was removed by gently wiping off with a filter paper. The specimen was vitrified by a rapid transfer into liquid ethane close to its freezing temperature. The examination of the sample was then performed with a Zeiss 902A electron microscope operating at 80 kV and 100K. The temperature of the specimen was kept below -165°C both during the transfer to the microscope and the examination. Images were recorded at under focus settings of about 2-3 μm to enhance the image contrast.

Results and discussions

We studied the microstructure of 0.5mM Clofarabine lipids dissolved in 50 mM PBS, as a function of time and of the thermal history of the sample, through DLS, CD and Cryo-TEM investigations. The samples were prepared by dissolving the dry powder in the buffer, through mild vortex-mixing. After having obtained a transparent solution, no further stirring was applied.

Time evolution of the lipidic self-assembly

Fig. 3 shows the time evolution of the Dynamic Light Scattering (DLS) and Circular Dichroism (CD) data for the two diastereomers freshly dissolved in PBS. The autocorrelation functions (Fig. 3A and 3B) can be fitted with a double exponential decay. Both modes are diffusive, as the linear trend of the deacay rates vs the squared scattering vector, reported in Fig. 2 reveals. These contributions are due to centre-of-mass motion of the aggregates.

The fast decay mode corresponds to a diffusion coefficient, which is identical for the two derivatives within experimental uncertainty ($D \approx 1.2 \times 10^{-7} cm^2 s^{-1}$, $R_H \approx 178$Å). The slow decay mode, due to larger aggregates, is different for the two diastereomers even in the freshly prepared samples ($D \approx 4.5 \times 10^{-8} cm^2 s^{-1}$, $R_H \approx 476$Å and $D \approx 2.6 \times 10^{-8} cm^2 s^{-1}$, $R_H \approx 824$Å for 1-2S and 1-2R, respectively).
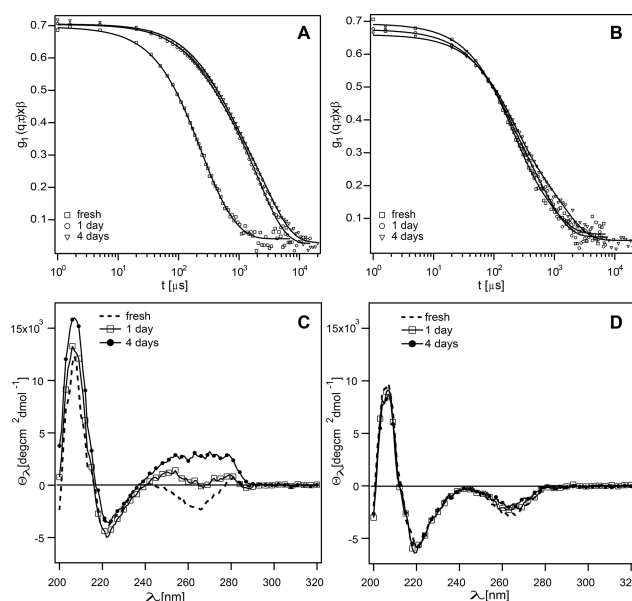
Fig. 3 Time evolution of DLS field autocorrelation functions and CD for **1-2S** and **1-2R** micellar solution. DLS field autocorrelation functions for A) **1-2S** and B) **1-2R** fresh micellar solutions (□), sample aged at 25°C for one day (○) and four days (∇). Solid curves are the best double-exponential fittings (equation 3) from which we extracted the characteristic decay modes (see text and Table 1). While the autocorrelation functions of the two fresh samples are very similar, **1-2S** show a dramatic change already after one day whereas for **1-2R** the change is less pronounced. C) and D) show the time evolution of the CD spectra of **1-2S** and **1-2R**, respectively, fresh micellar solution (dashed curve), sample aged one (□) and four (•) days at 25°C. **1-2S** shows a gradual change from fresh to four days while **1-2R** shows no change over the same time interval. All measurements were carried out at 0.5mM in 50mM PBS buffer at 25°C, the DLS measurements were made at θ=90.

The hydrodynamic sizes inferred from the diffusion coefficients indicate that, even for the faster decay, the aggregates cannot be accounted for by spherical micellar aggregates, (considering a monomer size of ~20 Å), but rather suggest the presence of elongated structures.

Table 1 Results obtained from the fitting of the field autocorrelation functions through equation 3 for fresh and aged samples of the two diastereoisomers at 25°C.

Sample	$D_1 [cm^2 s^{-1}]$	A_1	$D_2 [cm^2 s^{-1}]$	$R_{h1}[Å]^*$	$R_{h2}[Å]^*$
1-2S-fresh	1.2×10^{-7}	87%	4.5×10^{-8}	178.3	475.5
1-2R-fresh	1.2×10^{-7}	77%	2.6×10^{-8}	178.3	823.7
1-2S-2days	7.6×10^{-8}	33%	9.0×10^{-9}	281.6	2377.8
1-2R-2days	1.0×10^{-7}	70%	2.4×10^{-8}	214.0	891.7
1-2S-4days	7.6×10^{-8}	33%	9.0×10^{-9}	178.3	2377.8
1-2R-4days	1.1×10^{-7}	72%	1.54×10^{-8}	195.8	1389.2

*Hydrodynamic radii are only indicative since they were calculated through Stokes-Einstein relationship (equation 4), which gives the hydrodynamic radius of the equivalent diffusing sphere. Recall the complex structures of these self-assemblies, it is not possible to relate them to structural parameters.

Surprisingly, 1-2S aggregates show a noticeable evolution toward larger aggregates already after 24 hours and are then stable, while 1-2R has a much slower evolution, involving only the long-time decay, as reported in Fig. 3 and Table 1.

CD offers insight on base-base interaction pattern as the CD signal is sensitive to mutual interactions of the nucleobase analogs. The CD spectra of 1-2S (Fig. 3C) reveal a significant change over time, which suggests that the structural evolution observed in DLS is accompanied by a change in the base-base interaction pattern. Conversely, 1-2R does not show any significant change in the CD spectra over the time course of the experiment.
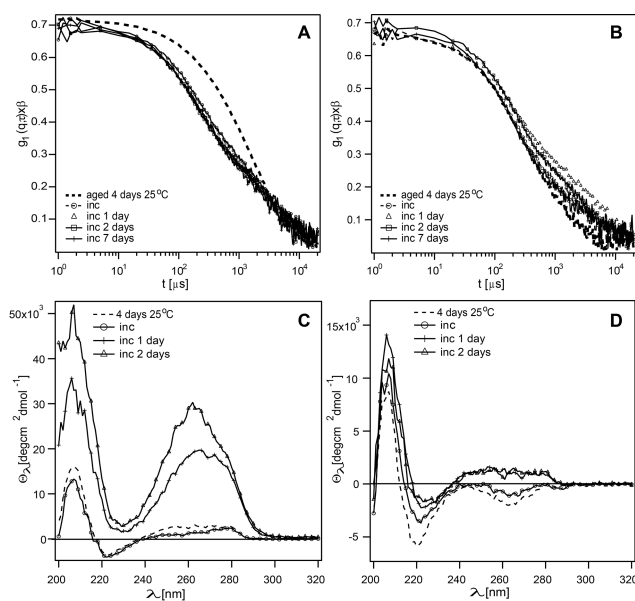
Fig. 4 Time evolution of DLS field autocorrelation functions and CD for **1-2S** and **1-2R** micellar solution after four days of aging at 25°C and two days of incubation at 45°C. DLS field autocorrelation functions for A) **1-2S** and B) **1-2R** after four days at 25°C (dashed lines), directly after incubation at 25°C for two days (o), after one day at 25°C after incubation (Δ), after two days at 25°C after incubation (♣) and seven days at after 25°C after incubation (+). CD spectra of C) **1-2S** and D) **1-2R** after four days at 25°C (dashed lines), directly after incubation at 25°C for two days (o), after one day at 25°C after incubation (+), after two days at 25°C after incubation (Δ). The incubation at 45°C has a strong affect on the **1-2S** as seen in the significant changes in both DLS and CD. Although the DLS and the CD changes also for **1-2R** after incubation the affect is significantly less pronounced. All measurements were carried out at 0.5mM in 50mM PBS buffer at 25°C, the DLS measurements were made at θ=90.

Thermal effects on the self-assembly

The effects of thermal cycles on the self-assembling properties of these derivatives were also investigated. In previous studies on the nucleolipid dilauroyl-phosphatidyl-adenosine (DLPA) we have shown that the thermal history of the sample has a dramatic effect on the resulting superstructures,[17] since temperature can promote the formation of long-lived non-equilibrium states. Incubation at 45°C for 48 hours drastically alters the structural features of 1-2S assemblies, as revealed both by DLS and CD (Fig. 4), i.e. of those aggregates which, upon ambient conditions, shows a stronger structural evolution. CD and DLS also change for 1-2R, but in a much less dramatic way when compared to 1-2S. To summarize, DLS highlights a complex self-assembly pattern, different time evolution of the structures and different thermal history behaviour.
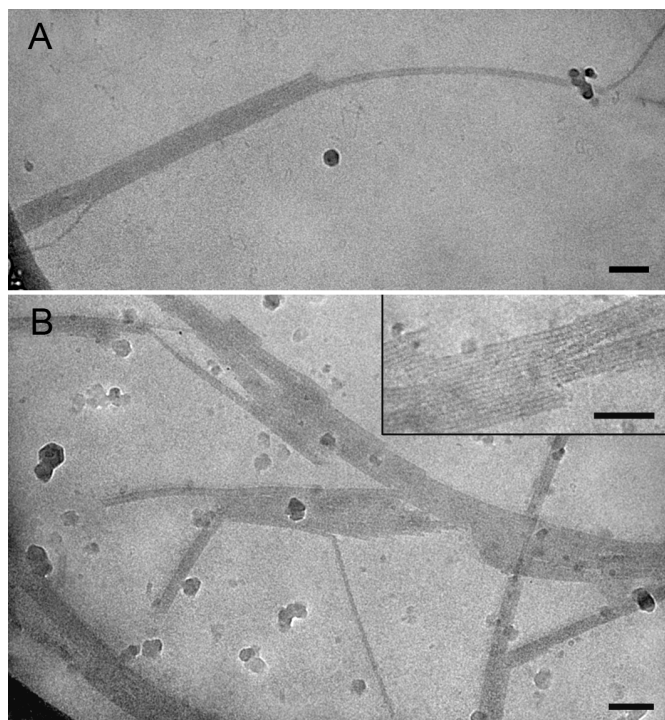
Fig. 5 Representative Cryo-TEM micrographs of 1-2S, 0.5mM in 50mM PBS, before (A) and after (B) incubation (48h incubation at 45°C). In both cases there are elongated threads, characterized by certain stiffness, occasionally aggregated through side-by-side interactions. In the aged samples before incubation smaller wormlike micelles are observed, while the incubated sample shows a higher supraorganization of these fibers to form stacked superstructures through side-side interactions. The length of the scale bar is 100nm.

Cryo-TEM investigation

Information on the morphology, flexibility and super-organization can be obtained by direct imaging of the aqueous aggregates by Cryo-TEM. Representative Cryo-TEM micrographs of 1-2S and 1-2R, both aged and incubated samples, are shown in Fig. 5 and 6, respectively. 1-2S (5A and 5B) shows extremely elongated threads, characterized by a notable stiffness, often associated through side-by-side interactions. The characteristic size of the thinner fibers is consistent with the monomer size, thus indicating that the primary aggregates are formed by cylindrical micelles. There are also small wormlike micelles visible in the background. Incubation increases the side-association in superaggregates, while it does not appear to reduce the stiffness. These results support the size variation observed in DLS as well as the change in base-base interaction pattern when the "primary" flexible wormlike micelles hierarchichally organize into superaggregated structure. This structural transition is accompanied by a change in base-base interactions, as the variation of CD patterns indicates for this derivative. Fig. 6 disclose a completely different behavior for 1-2R. The structures are characterized by a much higher degree of flexibility of the aggregates (6A and 6B), which can eventually

wind around to each other to form helicoidal superstructures with locally cylindrical curvature. Incubated samples display, in addition to twisted structures, elongated and apparently stiff, bilayer bands (Fig. 6C). The large degree of diversity in this sample makes both DLS and CD much more difficult to be interpreted.
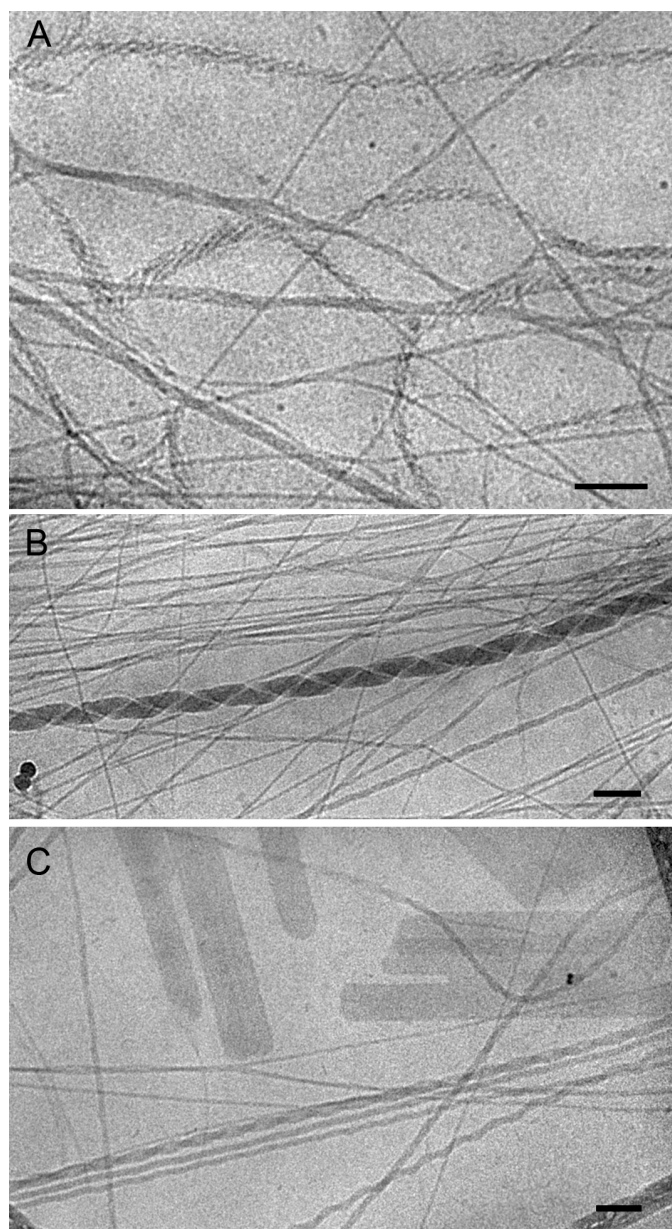
Fig. 6 Representative Cryo-TEM micrographs of **1-2R**, 0.5mM in 50mM PBS buffer, before (A-B) and after (C) incubation (48h incubation at 45°C). **1-2R** shows a very different self-assembling behaviour with respect to **1-2S**: the cylindrical curvature is kept but the fibers are much more flexible and tend to wound each other to form helicoidally superstructures which coexist with the starting structures. The temperature raise induces significant changes in the self-assembling behaviour with the coexistence of different superstructures such as twisted structures, fibers and elongated and apparently stiff bilayer bands. The length of the scale bar is 100nm.

Conclusions

The two nucleolipid diastereomers of 1 give rise to complex superstructures with different aggregation morphologies and sometime resulting in distinct interfacial curvatures. It is clear that, on the molecular scale, a different bending rigidity of the amphiphilic film, is responsible of the meso-scale behaviour. The different stereochemistry of the polar head results in a different flexibility of the aggregates, which in turn causes a completely different structural behaviour on a much higher length scale. These findings can be correlated with the difference in bioavailability and anti-tumor activity for the two diastereomers, administered at similar concentrations and conditions as those investigated in this study. In particular, the complex twisted aggregates formed by the 1-2R derivative (Fig. 6A and 6B) give rise to a lesser oral bioavailability and anti-tumor activity with respect to the more rigid structures formed by the 1-2S derivative. We hypothesize that the different morphologies, resulting from diastereselective self-assembly can definitely play a role and practically account for the different bioavailability. It is clear that a deeper investigation is needed to completely understand the chemical and biological mechanisms behind this effect.

This study highlights that a successful application of lipid pro-drugs as a means of drug delivery demands special attention to the self-aggregation behavior since very subtle structural features of the monomer can play a crucial role at mesoscopic scale which may seriously affect the therapeutic efficiency.

Notes and references

[a]Department of Chemistry; University of Florence and CSGI; Via della Lastruccia 3, Sesto Fiorentino, 50019 Florence Italy
[b]Department of Chemical and Biological Engineering, Chalmers University of Technology, Gothenburg, Sweden
[c]Centro Europeo di Nanomedicina c/o Dipartimento di Chimica, Materiali e Ingegneria Chimica G. Natta, Politecnico di Milano, Via Mancinelli 7, 20131 Milano, Italy
[d]School of Pharmacy, University of East Anglia, Norwich, NR47TJ, UK
[e]Heidelberg Pharma GmbH,, Schriesheimer Strasse 101, 68526 Ladenburg, Germany
[f]Department of Physical and Analytical Chemistry; Uppsala University; Box 579, S-75123 Uppsala, Sweden

1   http://www.accessdata.fda.gov/scripts/cder/ob/default.cfm

2   http://www.ema.europa.eu/ema/

3   E. Lech-Maranda, A. Korycka and T. Robak, Mini-Reviews in Medicinal Chemistry, 2009, 9, 805-812 805.

4   H.M.Kantarjian, V. Gandhi, P. Kozuch, S. Faderl, F. Giles, J. Cordes, S. O'Brien, N. Ibrahim, F. Khuri, M. Du, M.B. Rios, S. Jeha, P. McLaughlin, W. Plunkett, M. Keating, J. Clin. Oncol. 2003, 21, 1167-1173.

5   G.I.Neil, P.F. Wiley, R.C. Manak, T.E. Moxeley, Cancer Res. 1970, 30, 1047-1054.

6   J. Obermeier, G. Heckl-Oestreicher, C. Mueller, M. Kulke, R. Wehr, J. Anderl, Proceedings of the 100th Annual Meeting of the American Association for Cancer Research; 2009, Denver, CO: AACR 2009.

Abstract nr 4522; G. Heckl-Oestreicher, C. Mueller, C.Lutz, M. Kulke, J. Obermeier, A. Minchinton, R. Wehr, J. Anderl, Proceedings of the 100th Annual Meeting of the American Association for Cancer Research; 2009 Denver, CO: AACR 2009. Abstract nr 4523.

7   D. Berti, Current Opinion In Colloid & Interface Science, 2006, 11, 74.

8   D. Berti, C. Montis, P. Baglioni, Self-assembly of designer biosurfactants, Soft Matter, 2011, 7, 7150-7158.

9   M. Schade, D. Berti, D. Huster, A. Herrmann, A. Arbuzova, Advances in Colloid and Interface Science, 2014, 208, 235 -251

10   M. Banchelli, F. Betti, D. Berti, G. Caminati, F. Baldelli Bombelli, T. Brown, L. M. Wilhelmsson, B. Nordén and P. Baglioni, J. Phys.Chem. B, 2008, 112, 10942.

11   A. Gissot, M. Camplo, M. W. Grinstaff, P. Barthélémy, Org. Biomol. Chem., 2008, 6, 1324.

12   D. Berti, F. Baldelli Bombelli, M. Fortini, P Baglioni, Amphiphilic Self-assemblies Decorated by Nucleobases, J. Phys. Chem. B, 2007, 111,40, 11734 -11744.

13   P. Baglioni, D. Berti, Current Opinion in Colloid & Interface Science, 2003, 8, 55.

14   H. Hauser, BBA – Biomembranes; 1508, 1–2, 2000, 164–181.

15   F. Baldelli Bombelli, D. Berti, U. Keiderling, P. Baglioni, J.Phys.Chem. B, 2002, 106, 11613-11621.

16   J.D. Hartgerink, E. Beniash, S.I. Stupp, Science, 2001, 294, 1684-1688;

17   H. Cui , T. Muraoka, A.G. Cheetham, S.I. Stupp, Nano Lett. 2009, 9, 945-951

18   R. Oda, I. Huc, M. Schmutz, S.J. Candau, F.C. MacKintosh, Nature, 1999, 399, 566-569.

19   A. Brizard , C. Aime, T. Labrot, I. Huc, D. Berthier, F. Artzner, B. Desbat, R. Oda , J. Am. Chem. Soc. 2007, 129, 3754-3769.

20   F. Baldelli Bombelli, D. Berti, S. Milani, M. Lagi, P. Barbaro, G. Karlsson, A. Brandt, P. Baglioni, Soft Matter, 2008, 4, 1102-1113.

18   K. S. Ishaq, L. S.Kucera, S. L. Morris-Natschke, PCT WO1996006620 A2, 1996